RSC Advances

PAPER

View Article Online
View Journal | View Issue

Cite this: *RSC Adv.*, 2021, **11**, 33083

Preparation and characterization of a self-suspending ultra-low density proppant

Zhifeng Luo,[a] Jianbin Li,*[a] Liqiang Zhao,[a] Nanlin Zhang,*[a] Xiang Chen,*[a] Weijie Miao,[b] Weihua Chen[c] and Chong Liang[d]

A self-suspending ultra-low density proppant (UDP) was developed based on the polymerization of the unsaturated carbon double bond. Its performance was characterized by FT-IR and SEM, and the sphericity and roundness, diameter distribution, density, mechanical properties, the conductivity of the propped fracture, and mass loss of different fluids were measured. The test results indicated that the UDP no longer contained the unsaturated carbon double bond and the polymerization took place in the raw material. The fracture surface of UDP is compact and it is not easy to produce debris after compression failure. The sphericity and roundness of UDP were above 0.9, and the high sphericity and roundness provided high conductivity. The stirring speed has a great influence on the diameter of UDP, and the UDP with different sizes could be used to prop the hydraulic fracture to different widths. The average apparent density of UDP is as low as 1.044 g cm^{-3}, and it can be suspended in the fracturing fluid for a long time. The strain in the UDP is higher than that in the ceramsite and quartz sand, but its crushing ratio is far below theirs; therefore, the conductivity of the fracture propped by UDP was higher than that of quartz sand and ceramsite. The solubility of UDP in kerosene, reservoir water, and hydrochloric acid is below 1%, indicating that the UDP is also suitable for acid fracturing with proppant. All the experimental results proved that the self-suspending ultra-low density proppant has great potential use in hydraulic fracturing and acid fracturing.

Received 22nd July 2021
Accepted 4th September 2021

DOI: 10.1039/d1ra05611e

rsc.li/rsc-advances

1. Introduction

Hydraulic fracturing is often used in unconventional reservoirs to improve hydrocarbon recovery.[1–3] In the process of fracturing, the proppant serves as the most important material to avoid fracture closure.[4,5] Although proppants are widely used, there are two serious weaknesses: (1) with the continuous development of the deep reservoir, the proppant may break, deform, and embed under the high closure stress, resulting in the decrease of the hydraulic fracture width, which can not provide sufficient conductivity. (2) To carry high-strength proppant in fracturing treatment, it is necessary to use high-viscosity fracturing fluid, but high polymer concentration will lead to formation damage.

These disadvantages of fracturing proppants mentioned above are often responsible for fracture failure, which is in the process of construction and production, pollution, injury, blockage and other reasons caused the fracture conductivity to decrease continuously until the fracture failed.[6] Novel proppants have been proposed and developed to mitigate these problems. Hao *et al.* prepared a low-density ceramic proppant with calcined flint clay (45.6 wt% Al_2O_3) and solid waste coal gangue by solid-state sintering method; the low-density ceramic proppant sintered at 1400 °C had the best performance with bulk density of 1.27 g cm^{-3}, apparent density of 2.79 g cm^{-3}, breakage ratio of 3.27% under 35 MPa closed pressure and 8.36% under 52 MPa closed pressure.[7] Kincaid *et al.* proposed a self-suspending proppant in which conventional proppant particles are encapsulated with a thin layer of high-molecular-weight hydrogel polymer to form a self suspending proppant (SSP); once the SSP comes into contact with water, the hydrogel layer expands spontaneously and it forms a space-filling cushion around each granule, thereby increasing the volume of the particle and decreasing the particle density resulting in the reducing of settling rate of the proppant suspension.[8] Song *et al.* proposed a hydro-thermal reaction to form hydroxyapatite crystals on calcite-rich shale surfaces to act as proppants;[9] the most obvious defect of this method is its low conductivity. Chang *et al.* developed an *in situ* proppant generated from a fracturing fluid containing chemical precursors that will set into spherical particle beads; since the fracturing fluid is solid-

[a]*State Key Laboratory of Oil and Gas Reservoir Geology and Exploitation, Southwest Petroleum University, Chengdu 610500, China. E-mail: li15884539161@163.com; Nanlin_zhang@163.com; Chen_swpu@163.com*

[b]*Petroleum Engineering Technology Institute of Southwest Petroleum Branch, SINOPEC, Deyang 618000, China*

[c]*Engineering Technology Research Institute of Southwest Oil & Gas Field Company, PetroChina, Chengdu, Chengdu 610017, China*

[d]*Research Institute of Petroleum Exploration and Development, CNPC, Beijing 100083, China*

free, abrasion of the equipment due to the proppant is avoided.[10] J. D. Wine *et al.* performed numerous fracture design and production simulations, conductivity tests performed at 100 °F indicate organo-metallic crosslinked fracturing fluids yield significantly more conductivity impairment than borate crosslinked fluids.[11] Conductivity studies performed under *in situ* conditions by Penny have shown polymer loading, type of crosslinker, and breaker system dramatically affect the conductivity of a proppant pack.[12] Other proppants with different functions or performances have been developed for different oil and gas reservoirs, such as the low crushing rate proppant,[13] oil-wet proppant,[14] expandable proppant,[15] and non-spherical proppant.[16]

Existing proppants have addressed some problems, but the density and suspension ability do not meet the requirement of network fracturing. It is difficult to fully prop the hydraulic fracture network. With the development of the petroleum industry, oil and gas exploration aims at extraction from shallow layers to deep layers, and from low closure pressure to high and ultra-high closure pressure. The requirement of increasing the proppant strength causes a concomitant increase in proppant density, and finally causes the consequences that the proppants settle rapidly near the well.[17] Therefore, it is necessary to carry out the research and development of high-strength and low-density proppants to improve the fracturing effect. In this study, we describe a self-suspending ultra-low density proppant, which may be used as a novel fracturing treatment agent.

2. Experimental section

2.1 Materials

The materials needed for UDP production are as follows:[18]

Paraxylene (PX); acrylonitrile (AN); hydrogen peroxide (HP, $\omega_{H_2O_2}$ = 35%); ferrous sulfate (FS); 1,3,5-tri-2-propenyl-1,3,5-triazine-2,4,6(1*H*,3*H*,5*H*)-trione (TAIC); vinyl acetate (VA).

A typical preparation method is as follows:

(1) 50 g PX, 12 g VA and 2 g AN are added into the beaker and stirred until they are completely dissolved at room temperature (25 °C);

(2) 2 g HP solution is added to the beaker and stirred until it is fully mixed;

(3) In another beaker, take 10 g TAIC, heat it in a water bath at 40 °C, and slowly add the solution prepared in the previous step while stirring;

(4) 2 g FS is added to the solution prepared in step (3), name the mixture liquid MX, and stirred until the self-suspending spherical ultra-low density proppant (UDP) particles are formed.

2.2 Fourier transform infrared (FT-IR) measurements

The Fourier Transform Infrared (FT-IR) spectra of UDP and the liquid mixture before the generation of UDP are tested with a WQF-520A Fourier transform infrared spectrometer. The test method is as follows: drop the mixed liquid onto a piece of KBr sheet and spread it evenly on the sheet surface. The FT-IR test can be carried out using this sample. Use pure spectral KBr and UDP to prepare a mixture with the mass ratio (KBr : UDP = 50 : 1), mix it evenly, grind, and roll into thin slices. Their infrared spectrum is measured by a WQF-520A Fourier transform infrared spectrometer at room temperature.

2.3 SEM measurements

The morphology of MX was investigated by an FEI Quanta 450 ESEM (environmental scanning electron microscope). MX was frozen using liquid nitrogen. The frozen surfaces of the samples were observed with ESEM operating at an accelerating voltage of 20 kV.

Besides, the morphology of UDP was investigated using the FEI Quanta 450 environmental scanning electron microscope.

2.4 Density tests of UDP

The density of UDP determines its suspension performance and its ability to be carried by the fracturing fluid. The lower the density, the easier it is to be carried by the fracturing fluid, and the easier it is to enter the far end of the fracture to improve the conductivity there. The density includes both apparent density and bulk density. The test method for apparent density is as follows:

(1) Use a balance with a sensitivity of 0.0001 g to weigh the mass m_1 of the dry empty density bottle;

(2) Fill the density bottle with water and weigh its mass m_2;

(3) Empty the density bottle and dry it;

(4) Fill the density bottle with ethanol and weigh its mass m_3;

(5) Measure out an appropriate amount of UDP. The mass is equal to m_4;

(6) Pour out approximately half of the ethanol in the density bottle, and move the UDP in step (5) to the density bottle;

(7) Fill the density bottle with ethanol and rotate it along the vertical axis until all bubbles in the density bottle are discharged. If necessary, refill the bottle with ethanol, and weigh the mass m_5.

The calculated equation of apparent density is:

$$\rho_s = \frac{m_4}{\frac{m_2 - m_1}{\rho_w} - \frac{(m_2 - m_1)(m_5 - m_4 - m_1)}{\rho_w(m_3 - m_1)}} \quad (1)$$

where, ρ_s is the apparent density of UDP, g cm^{-3}; ρ_w is the density of water, g cm^{-3}.

The method for measurement of bulk density is:

(1) Take a balance of sensitivity 0.0001 g to weigh the mass m_7 of the empty brass cylinder of Q/SY-2 bulk density meter (Fig. 1);

(2) Close the outlet of the funnel with a rubber ball valve, center the brass cylinder directly below the outlet of the funnel, and pour the UDP sample into the funnel from the beaker;

(3) Open the rubber ball valve at the bottom of the funnel, pour the UDP samples into the brass cylinder from the funnel, and use a ruler to smoothen it at the edge of the cylinder, so that the sample is flush with the surface of the brass cylinder mouth;

(4) The weight of the brass cylinder and the sample in the cylinder is m_8.

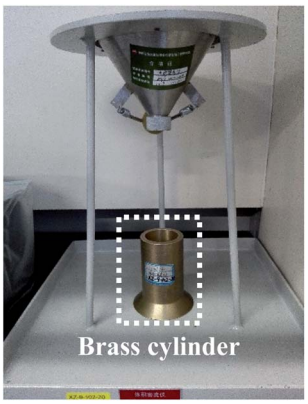

Fig. 1 Q/SY-2 bulk density meter.

The bulk density is calculated using the equation:

$$\rho_h = \frac{m_8 - m_7}{V} \quad (2)$$

where ρ_h is the bulk density of UDP, g cm^{-3}; V is the nominal volume of the brass cylinder, cm^3.

2.5 Sphericity and roundness of UDP measurements

The morphology of UDP was characterized by the ICM (image collecting microscope) shown in Fig. 2. Then, process the image taken by the ICM and extract the edges of all proppant particles in the image, the roundness and sphericity are measured based on the edges. The sphericity was measured qualitatively according to the ISO 13503-2-2006 standard (Fig. 3) based on the image taken by the ICM.

2.6 Diameter measurements of UDP

The particle size of UDP determines the width of a hydraulic fracture into which it can enter and how suitable it is for fracturing. Once the raw material ratio of UDP is determined, its diameter is only related to the stirring speed. Therefore, the particle size distribution under different stirring speeds is tested.

Fig. 2 Image collecting microscope.

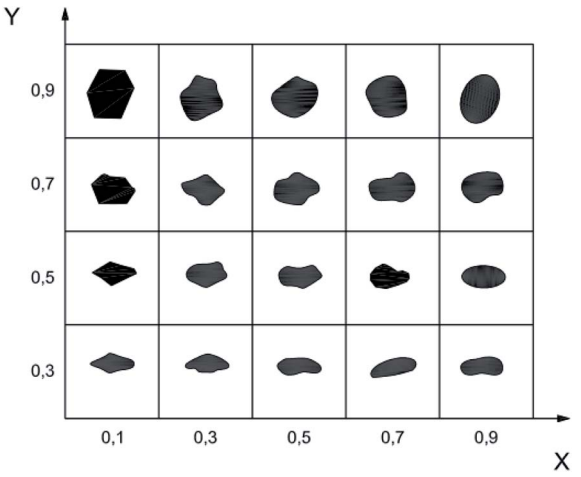

Fig. 3 Chart for visual estimation of sphericity and roundness in ISO 13503-2-2006 (*X*-roundness, *Y*-sphericity).

2.7 Mechanical property test

Under the high closure pressure in the hydraulic fracture, UDP may break and embed into the formation rock, resulting in a decrease in the conductivity of the propped fractures. Hence, it is necessary to test the compressive strength of UDP. The strain of the UDP under different pressures and the long-term strain under 55 MPa were tested with the experimental device shown in Fig. 4. The strains in ceramsite, quartz sand, and UDP under different pressures were compared.

The test method for compressive strength is as follows:

(1) Prepare an equal amount of ceramsite, quartz sand and UDP respectively, and use the compressive strength test device shown in Fig. 4 to gradually pressurize to 55 Mpa;

(2) Measure the strain values of ceramsite, quartz sand and UDP under different stresses;

(3) Prepare equal amounts of 40/70 mesh quartz sand, 20/40 mesh quartz sand, 20/40 mesh ceramsite and UDP, and gradually pressurize them to 60 Mpa;

(4) Screening, weighing and calculating the crushing rate under different stresses;

(5) Prepare a certain amount of UDP, and pressurize it stably at 55 Mpa;

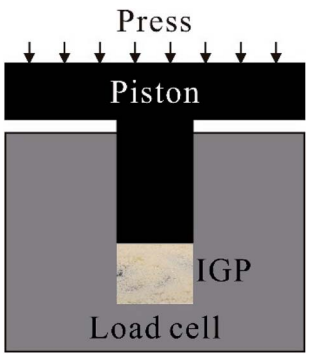

Fig. 4 Experimental device to test the compressive strength.

Fig. 5 Proppant cell in the conductivity test device.

Fig. 6 Conductivity test device.

(6) Measure UDP strain values at different times.

2.8 Fracture conductivity

The conductivity of the propped-fracture is the key parameter in evaluating the effect of fracturing. Under high closure pressure, the conductivity and proppant concentration vary greatly, making testing imperative. According to SY/T6302-2009,[19] the conductivity test steps are shown as follows:

(1) The set mass of UDP, quartz sand, and ceramsite was subjected to the proppant cell (Fig. 5) of the conductivity test device (Fig. 6), respectively.

(2) The closure pressure was set to a different value, respectively.

(3) The outlet flow under each test pressure, the left and right width of the propped fracture, and the reading of the differential pressure transmitter were recorded, the fracture conductivity value was calculated using eqn (3).

$$kW_f = \frac{6.4499\ \mu m}{\rho(I - I_{min})} \quad (3)$$

where kW_f is the conductivity value, μm^2 cm; m is the outflow liquid quality every 2 min, g/2 min; μ is the viscosity of the liquid used to test the conductivity, mPa s; ρ is the density of the liquid used to test the conductivity, g cm^{-3}; I is the reading of the differential pressure transmitter, mA; I_{min} is the initial reading of the differential pressure transmitter, mA, equal to 4 mA.

2.9 Mass loss rate tests in different fluids

After UDP enters the hydraulic fracture, it will be in high temperature and high-pressure fluid environment for a long time. The physical and chemical stability in the formation fluid environment directly determines the long-term fracturing effect. Therefore, it is necessary to test the mass loss of UDP in crude oil and reservoir water. To facilitate the analysis, the mass loss rate of UDP is tested with kerosene and reservoir water respectively.

(1) UDP with a mass of m_0 is put in the reaction kettle and diesel or reservoir water with a mass of m' is added;

(2) The reaction kettle is sealed and placed in an electric oven, and the temperature is set to 120 °C;

(3) After 48 h, take out the reaction kettle, dry the UDP at 80 °C for 6 h, and weigh its mass m.

The mass-loss rate is calculated by:

$$\eta = \frac{m_0 - m}{m_0} \times 100\% \quad (4)$$

where η is the mass-loss rate, %.

The proppant and acid may be used together in hydraulic fracturing. The proppant is used to support hydraulic fractures,

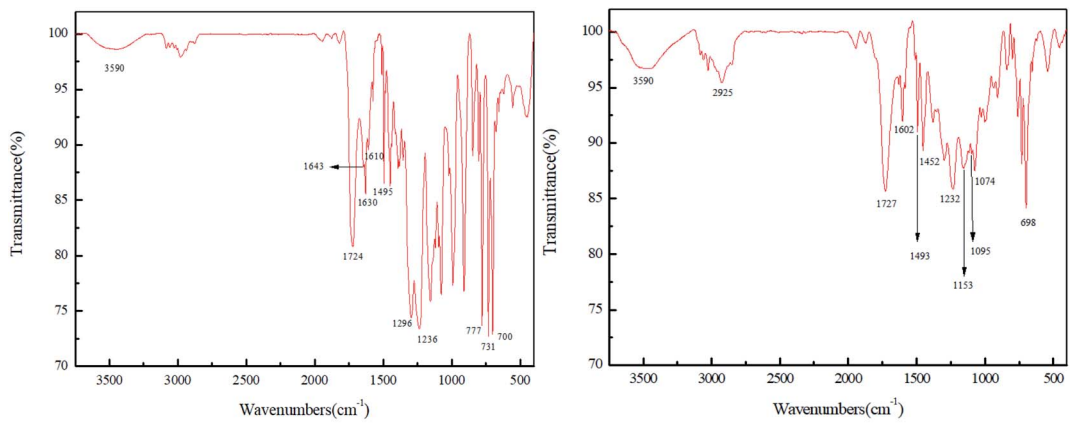

Fig. 7 FT-IR spectra of UDP.

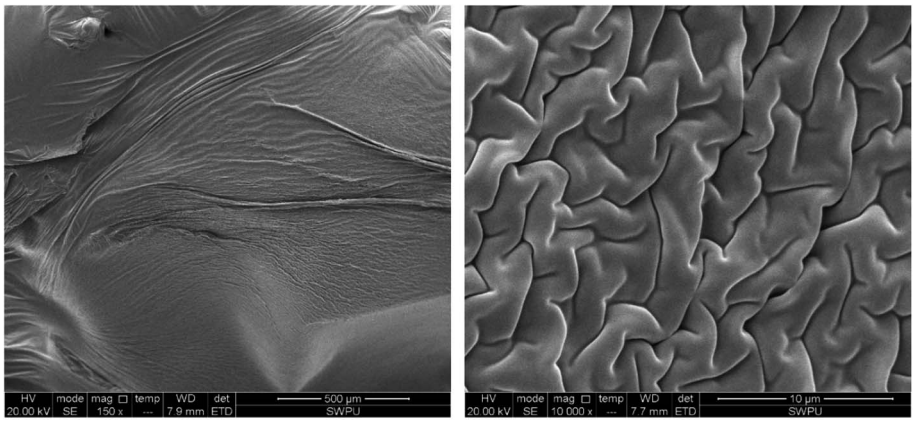

a）×150 b）×10000

Fig. 8 MX microstructures.

and acid is used to break the fracturing fluid or remove carbonate plugs.[20] Therefore, it is necessary to test the mass loss rate of UDP in the acid solution. The mass-loss rate of UDP in 20% hydrochloric acid was tested by the method mentioned above.

3. Results and discussions

3.1 FT-IR measurements

3.1.1 Results. The FT-IR spectra of MX and UDP are shown in Fig. 7.

3.1.2 Discussions. In Fig. 7a, the obvious characteristic absorption peaks at 1724 cm^{-1} and 1236 cm^{-1} are C═O and C–O respectively, indicating that there are a large number of ester groups in the molecular chain; the characteristic absorption peaks of C═C are found at 1630 cm^{-1} and 1643 cm^{-1}, indicating that there are two kinds of C═C in the MX, namely, the C═C from the TAIC and the VA. There is a wide peak at approximately 3590 cm^{-1}, which is the stretching vibration peak of –OH, and there is an obvious absorption peak at 1296 cm^{-1}, which is the stretching vibration peak of C–O in primary alcohol.

In Fig. 7b, there is a wide peak at approximately 3590 cm^{-1}, which is the stretching vibration peak of –OH. The obvious characteristic absorption peaks at 1727 cm^{-1} and 1232 cm^{-1} were C═O and C–O, indicating the presence of the ester group in the molecular chain. No obvious absorption peak was found in the range of 1620–1680 cm^{-1}, indicating that unsaturated carbon double bond was no longer contained in the UDP and the polymerization took place between TAIC and the VA.

3.2 SEM measurements

3.2.1 Results. Fig. 8 and 9 show the microstructures of MX and UDP, respectively.

3.2.2 Discussions. Fig. 8 shows that MX is a homogeneous fluid, and there is no three-dimensional network macromolecule similar to conventional polymer fracturing fluid, which indicates that there is good compatibility between the AN, TAIC, and VA. Fig. 9 shows that the morphology of the UDP fracture surface is different from that of conventional ceramsite

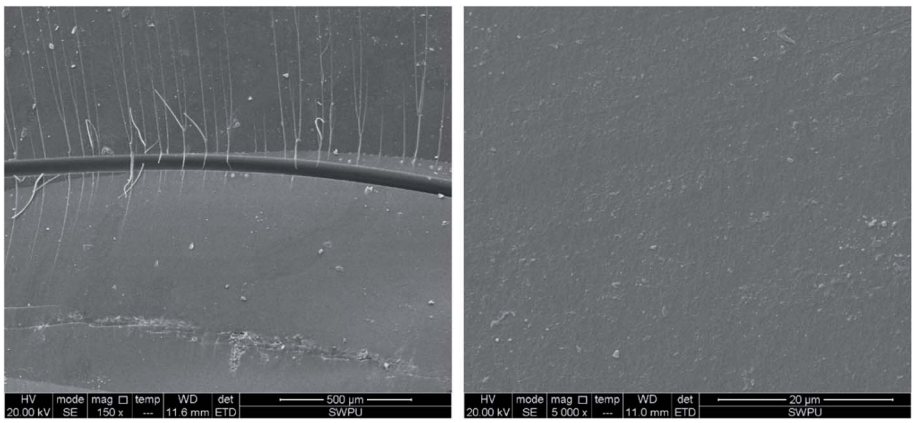

a）×150 b）×5000

Fig. 9 UDP fracture surface microstructures.

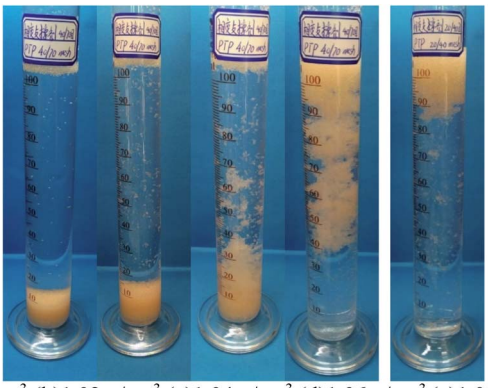

(a)1 g/cm^3 (b)1.02 g/cm^3 (c)1.04 g/cm^3 (d)1.06 g/cm^3 (e)1.08 g/cm^3

Fig. 10 The UDP suspended in the KCl solution with different density.

Table 1 Density test results

Item	No. 1	No. 1	No. 1	Average
Apparent density (g cm^{-3})	1.044	1.042	1.045	1.044
Bulk density (g cm^{-3})	0.671	0.638	0.655	0.655

proppant. UDP is relatively compact in texture, the fracture surface is very flat and smooth, and the stress crack is very straight. Therefore, UDP does not easily produce debris after compression failure, which can provide higher conductivity under high closure stress.[21]

3.3 Density of UDP

3.3.1 Results. The apparent density and bulk density were tested three times respectively, and the average value was calculated, as shown in Table 1.

The average apparent density of UDP is approximately 1.044 g cm^{-3}, and the bulk density is approximately 0.655 g cm^{-3}. The bulk density of UDP is close to that of water. Fig. 10 shows the UDP suspended in KCl solutions with different densities. UDP was nearly suspended in the KCl solution with a density of 1.04 g cm^{-3}. When the density of the KCl solution increased to 1.08 g cm^{-3}, UDP was completely suspended in the solution. The density of the fracturing fluid is usually more than 1.1 g cm^{-3}, so that UDP can remain in suspension and effectively improve the fracturing effect. The density of UDP is lower than the existing low-density proppant.[7,22–27]

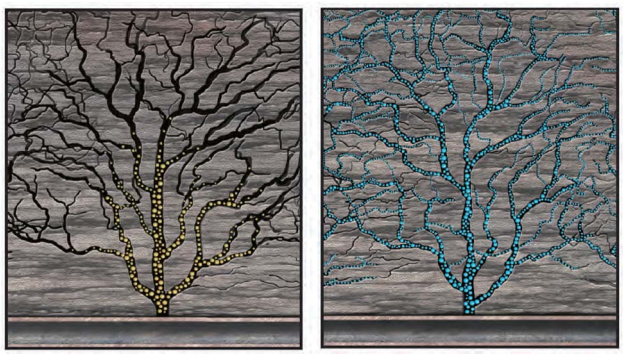

(a) Conventional proppant (b)Low-density proppant

Fig. 11 Prop effect of conventional proppant and low-density proppant.[28]

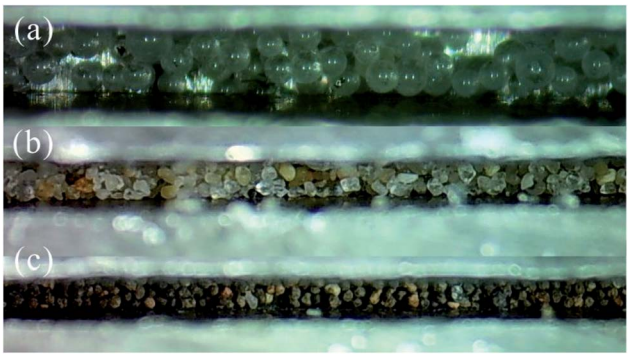

Fig. 12 The morphology images of UDP, quartz sand and ceramsite.

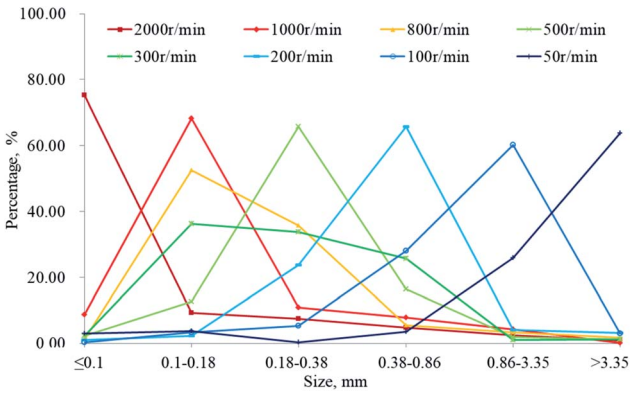

Fig. 13 Size distribution of UDP at different stirring speeds.

3.3.2 Discussions. The low density ensures that UDP can be suspended in the fracturing fluid, and improve its migration distance, thereby improving the fracturing effect.[29] Fig. 11 shows the prop effect of conventional proppant and low-density proppant.[30] The conventional proppant is of high density, settles easily, and is difficult to carry to the far front of the

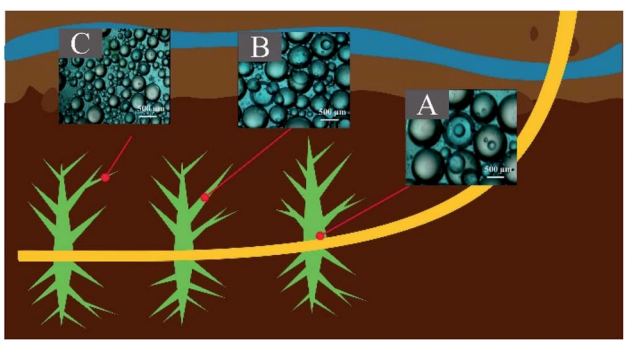

Fig. 14 Hydraulic fracture propped with UDP of different size.

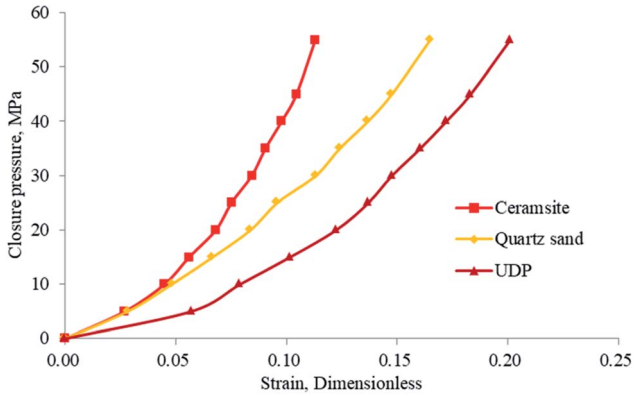

Fig. 15 Strain of different proppant at different closure pressures.

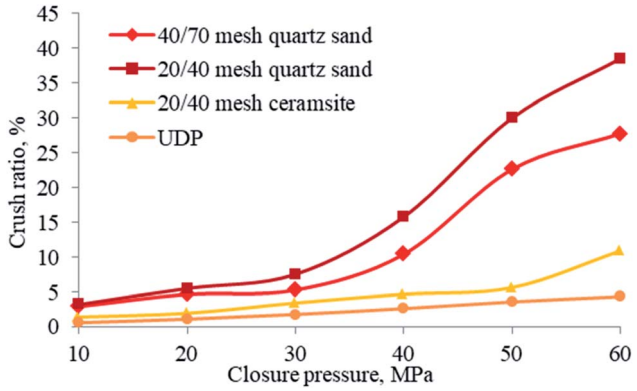

Fig. 16 Crushing ratio of different proppant at different closure pressures.

fracture, while the low-density proppant can be easily carried to the tip of the fracture, which ensures that the tip of the fracture is also propped and the fracturing effect is significantly improved.

3.4 Sphericity and roundness of UDP

3.4.1 Results. The morphology of the UDP is shown in Fig. 12. The surface of the UDP was smooth (Fig. 12a). By comparison, the morphologies of quartz sand and ceramsite showed a rough surface (Fig. 12b and c).

3.4.2 Discussions. Referring to Fig. 3, the sphericity and roundness of UDP were above 0.9, which is better than quartz sand (0.7) and ceramsite (0.8). Good sphericity and roundness provide high conductivity.[23,31]

3.5 Diameter distribution

3.5.1 Results. Fig. 13 shows the size distribution of UDP at different stirring speeds. The diameter of UDP is mainly distributed between 0.1 and 3.35 mm. Under different stirring speeds, the distributions of UDP diameter are different, and the stirring speed has a great influence on the diameter. The greater the mixing speed, the smaller the UDP diameter. On the contrary, the smaller the mixing speed, the larger the UDP diameter.

3.5.2 Discussions. Multi-size UDP can be used to support cracks with different crack widths and improve the propping effect. A smaller size proppant results in a larger propped fracture surface area and using large proppant particles results in a high average fracture conductivity.[32] As shown in Fig. 14, large, medium, and small UDP particles could be injected at three stages to prop the wide main body (A) of the fracture, medium width primary branch fracture (B), and narrow secondary branch fracture (C) in network fracturing.

3.6 Mechanical properties

3.6.1 Results. Fig. 15 shows the strain of various proppants. Fig. 16 shows the crushing ratio of different proppant at different closure pressures. Fig. 17 shows the micrograph of UDP fragmentation at different closure pressures. Fig. 18 shows the width of the propped fractures at different times under 55 MPa closure stress.

3.6.2 Discussions. A fracture containing large proppants more readily closes during the production process, and the closing pressure has a considerable effect on the proppant rock mechanical parameters.[33] The strain of UDP was higher than that of ceramsite and quartz sand. Higher strain led to

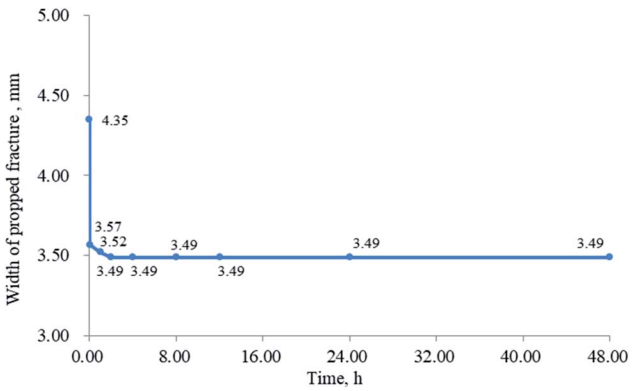

Fig. 18 Width of propped fracture at different time.

Fig. 17 Fragmentation of UDP at different closure pressures.

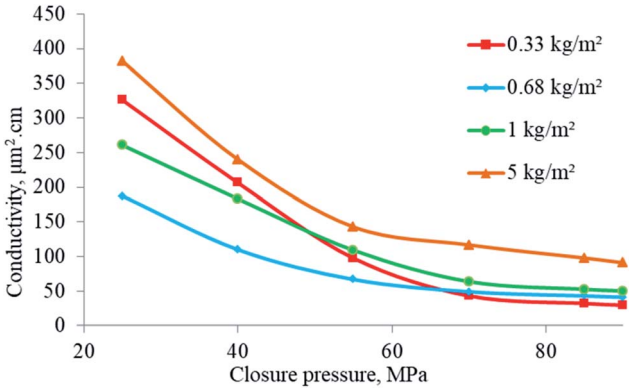

Fig. 19 Conductivity test results under different concentrations.

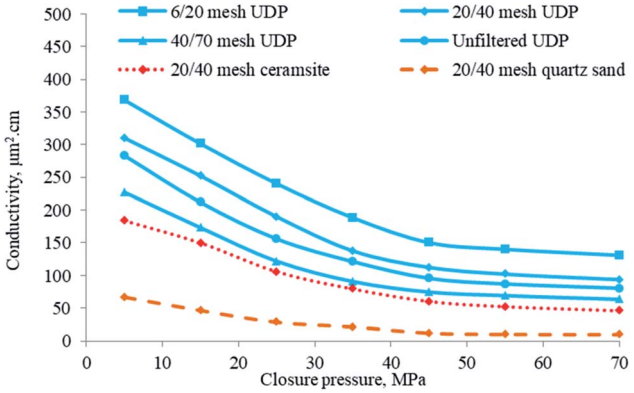

Fig. 20 Conductivity test results of different types of proppant.

(a) Kerosene; (b) Reservoir water; (c) Hydrochloric acid

Fig. 21 The UDP in different fluids.

a decrease in the propped fractures (Fig. 15). But since the crushing ratio of UDP was far below that of ceramsite and quartz sand (Fig. 16), blocking can be effectively avoided by proppant fragmentation. Under the pressure of 30 MPa, no fragmented UDP was observed. When the closure pressure increased to 55 MPa, some fragmentation was observed (Fig. 17).

The effect of stress on the fracture width is significant.[34] The width of the propped fracture decreased rapidly during the first 0.04 h. Subsequently, the decrease tended to be slow and continued to be the same for 2 hours (Fig. 18). The test results indicated that UDP exhibited long-term stability, maintained good propping performance, and a long-term high conductivity under 55 MPa closure stress. Through the analysis of fracture width, the best viscosity parameters of fracturing fluid are obtained, and the fracturing fluid is optimized.[35]

3.7 Fracture conductivity

3.7.1 Results. Fig. 19 shows the results of the conductivity test under different concentrations of UDP at 0.33 kg m^{-2}, 0.68 kg m^{-2}, 1 kg m^{-2}, and 5 kg m^{-2} respective to the single-layer-partially propped, single-layer propped, double-layer, and multi-layer propped conditions. Fig. 20 shows that the conductivity was directly proportional to the UDP particle size.

3.7.2 Discussions. The conductivity of the propped fracture increased with an increase in the UDP concentration between 0.68 kg m^{-2} to 5 kg m^{-2} (Fig. 19). Under the condition of single-layer partial prop, the space that was not occupied by UDP provided more channels for fluid flow, and the conductivity was higher than other experimental conditions. However, due to the breakage and deformation of UDP, the single-layer partial prop had no advantage over other experimental conditions under high closure pressure.

Due to the low crushing ratio and high sphericity, the conductivity of the fracture propped by UDP was higher than that of quartz sand and ceramsite (Fig. 20).

3.8 Mass loss rate in different fluids

3.8.1 Results. Table 2 shows the mass of UDP before the test and after the test. Fig. 21 shows the UDP in different fluids.

3.8.2 Discussions. The mass-loss rate in kerosene, reservoir water, and hydrochloric acid are 1.0%, 0.8%, and 0.2%, respectively. The mass-loss rate is low and meets the fracturing requirements. It is confirmed that the UDP can be kept stable in the fluid environment of the reservoir and provide long-term conductivity. Besides, the solubility of UDP in hydrochloric acid is low, which is suitable for acid fracturing with the proppant.

Table 2 Mass loss rate of UDP in different fluids

Item	Mass of UDP before the test, g	Mass of UDP after the test, g	Mass loss rate
Kerosene	5	4.95	1.0%
Reservoir water	5	4.96	0.8%
Hydrochloric acid	5	4.99	0.2%

3.9 Proppant embedment

After stimulating a well, the conductivity and porosity of the well will decline because of proppant embedment as well as deformation.[36] Particle shapes also affect the overall mechanical behavior and embedment of proppant pack in fractures.[37] Proppants appear to undergo substantial proppant pack compaction and porosity reduction due to the strong *in situ* confining stresses that occur underground.[38] The embedment of proppants leads to the decrease of conductivity. However, the fracture conductivity test has shown that the conductivity of UDP propped fracture is higher than that of quartz sand and ceramsite under high closing stress. This shows that the UDP embedding amount is small.

4. Conclusions

A self-suspending ultra-low density proppant (UDP) was developed based on the polymerization between the unsaturated carbon double bonds. Its performance was characterized by FT-IR, SEM, as well as the measurement of sphericity and roundness, diameter distribution, density, mechanical property, the conductivity of propped fracture, and mass loss in different fluids. The test results indicated that the average apparent density of UDP is as low as 1.044 g cm^{-3} and the low density makes it easy for the proppant to be carried to the tip of the hydraulic fracture, which ensures that the tip of the fracture is also propped and this significantly improves the fracturing effect. Besides, the sphericity and roundness, mechanical properties, and conductivity of UDP are better than that of ceramsite and quartz sand, and the acid resistance performance indicates that the UDP is also suitable for acid fracturing with the proppant. All experimental results indicate that the self-suspending ultra-low density proppant has great potential for use in hydraulic fracturing and acid fracturing.

Funding sources

This work was supported by the National Natural Science Foundation of China (51974264), the Research and Innovation Fund for Graduate Student of Southwest Petroleum University (2019CXZD018).

Author contributions

The manuscript was written through the contributions of all authors. All authors have given approval to the final version of the manuscript. These authors contributed equally.

Conflicts of interest

The authors declare no competing financial interest.

References

1 Y. Hu, J. Zhao, J. Zhao, C. Zhao, Q. Wang, X. Zhao and Y. Zhang, Coiled tubing friction reduction of plug milling in long horizontal well with vibratory tool, *J. Pet. Sci. Eng.*, 2019, **177**, 452–465.
2 P. Liu, F. Liu, C. She, L. Zhao, Z. Luo, W. Guan and N. Li, Multi-phase fracturing fluid leakoff model for fractured reservoir using extended finite element method, *J. Nat. Gas Sci. Eng.*, 2016, **28**, 548–557.
3 J. Zhao, Q. Wang, Y. Hu, L. Ren and C. Zhao, Numerical investigation of shut-in time on stress evolution and tight oil production, *J. Pet. Sci. Eng.*, 2019, **179**, 716–733.
4 D. Fjaestad and I. Tomac, Experimental investigation of sand proppant particles flow and transport regimes through narrow slots, *Powder Technol.*, 2019, **343**, 495–511.
5 N. Li, J. Li, L. Zhao, Z. Luo, P. Liu and Y. Guo, Laboratory Testing on Proppant Transport in Complex-Fracture Systems, *SPE Prod. Oper.*, 2017, **32**(4), 382–391.
6 Y. Liu, Z. Zhang, F. Gao, Y. Liu and X. Zhang, Fracture failure and its influence on well productivity in low permeability reservoir[A], *2018 IFEDC International Conference on Exploration and Development of Oil and Gas Fields[C]*, Xi 'an Petroleum University, Shaanxi Petroleum Institute: Xi 'an Huaxian Network Information Service Co., Ltd., 2018, p. 9.
7 J. Hao, H. Hao, Y. Gao, X. Li, M. Qin and K. Wang, Effect of Sintering Temperature on Property of Low-Density Ceramic Proppant Adding Coal Gangue, *Mater. Sci.*, 2020, **26**(1), 94–98.
8 K. P. Kincaid, P. M. Snider, M. Herring, R. P. Mahoney and D. Soane, Self-Suspending Proppant, in *SPE Hydraulic Fracturing Technology Conference*, Society of Petroleum Engineers: The Woodlands, Texas, USA, 2013, pp. 1–12.
9 S. Tong, C. Miller and K. Mohanty, Generation of In-Situ Proppant through Hydro-Thermal Reactions, in *SPE Hydraulic Fracturing Technology Conference and Exhibition*, Society of Petroleum Engineers: The Woodlands, Texas, USA, 2019, pp. 1–13.
10 F. F. Chang, P. D. Berger and C. H. Lee, *In-Situ* Formation of Proppant and Highly Permeable Blocks for Hydraulic Fracturing, in *SPE Hydraulic Fracturing Technology Conference*, Society of Petroleum Engineers: The Woodlands, Texas, USA, 2015, pp. 1–11.
11 J. D. Wine, M. P. DeBonis and R. L. Thomas, The Effect of Guar and HPG Crosslinked Fracturing Fluids on Well Performance: A Case Study, *paper presented at the Low Permeability Reservoirs Symposium*, Denver, Colorado, March 1989.
12 G. S. Penny, An Evaluation of the Effects of Environmental Conditions and Fracturing Fluids Upon the Long-Term Conductivity of Proppants, *paper SPE 16900 presented at the 1987*, SPE Annual Technical Meeting, Dallas, TX, Sept. 27-30.
13 X. Ren, Q. Hu, X. Liu, Y. Shen, C. Liu, L. Yang and H. Yang, Nanoparticles Patterned Ceramsites Showing Super-Hydrophobicity and Low Crushing Rate: The Promising Proppant for Gas and Oil Well Fracturing, *J. Nanosci. Nanotechnol.*, 2019, **19**(2), 905–911.
14 T. Palisch, M. Chapman and J. Leasure, Novel Proppant Surface Treatment Yields Enhanced Multiphase Flow Performance and Improved Hydraulic Fracture Clean-up,

in *SPE Liquids-Rich Basins Conference - North America*, Society of Petroleum Engineers: Midland, Texas, USA, 2015, pp. 1–11.

15 L. Santos, A. Dahi Taleghani and G. Li, Expandable proppants to moderate production drop in hydraulically fractured wells, *J. Nat. Gas Sci. Eng.*, 2018, **55**, 182–190.

16 J. Xu, Y. Ding, L. Yang, Z. Liu, R. Gao, H. Yang and Z. Wang, Conductivity analysis of hydraulic fractures filled with nonspherical proppants in tight oil reservoir, *Energy Sci. Eng.*, 2020, **8**(1), 166–180.

17 S. Shiozawa and M. McClure, Simulation of proppant transport with gravitational settling and fracture closure in a three-dimensional hydraulic fracturing simulator, *J. Pet. Sci. Eng.*, 2016, **138**, 298–314.

18 Z. Luo, L. Wu, L. Zhao, N. Zhang, C. Zhou, H. Liu, P. Liu, N. Li, N. Li, J. Liu, Y. Geng, Y. Zhang and D. Ren, A production method of ultra-low density proppant based on supramolecular materials, CN 110511306A, 2019-11-29.

19 National_Energy_Board_of_China, *SY/T 6302-2009 Recommended practices for evaluating short term proppant pack conductivity*, Petroleum Industry Press, 2009.

20 P. Karadkar, W. Suzart, A. Sabhapondit, A. Buenrostro and J. L. Jauregui, Novel High Viscus Acid System for Proppant Fracture Acidizing, in *Abu Dhabi International Petroleum Exhibition & Conference*, Society of Petroleum Engineers, Abu Dhabi, UAE, 2016, p. 10.

21 C. Zhang, L. Zhao, D. Yu, G. Liu, Y. Pei, F. Huang and B. Liu, The evaluation on physical property and fracture conductivity of a new self-generating solid proppant, *J. Pet. Sci. Eng.*, 2019, **177**, 841–848.

22 J. Fan, T. P. Bailey, Z. Sun, P. Zhao, C. Uher, F. Yuan and M. Zhao, Preparation and properties of ultra-low density proppants for use in hydraulic fracturing, *J. Pet. Sci. Eng.*, 2018, **163**, 100–109.

23 X. Han, Q. Cheng, F. Bao, J. Gao, Y. Yang, T. Chen, C. Yan and R. Ma, Synthesis of Low-Density Heat-Resisting Polystyrene/Graphite Composite Microspheres Used as Water Carrying Fracturing Proppants, *Polym.-Plast. Technol. Eng.*, 2014, **53**(16), 1647–1653.

24 G. Li, X. Chang, B. Zhu, K. Wang, Y. Zhou, Y. Wu, Y. Tian and P. Bai, Sintering mechanism of high-intensity and low-density ceramic proppants prepared by recycling of waste ceramic sands, *Adv. Appl. Ceram.*, 2019, **118**(3), 114–120.

25 R. Ma, W. Tang, P. Hu and T. Chen, Fabrication of low-density heat-resistance polystyrene/carbon black composite microspheres used as hydraulic fracturing proppant, *Mater. Express*, 2019, **9**(2), 150–158.

26 X. Ma, Y. Tian, Y. Zhou, K. Wang, Y. Chai and Z. Li, Sintering temperature dependence of low-cost, low-density ceramic proppant with high breakage resistance, *Mater. Lett.*, 2016, **180**, 127–129.

27 J. Zhao, Z. Liu and Y. Li, Preparation and characterization of low-density mullite-based ceramic proppant by a dynamic sintering method, *Mater. Lett.*, 2015, **152**, 72–75.

28 G. Xinjun, W. Minsheng, H. Fuwei and G. Lidong, Proppants for Fracturing Fluids: New Progress Made and Direction of Future Development, *Drill. Fluid Completion Fluid*, 2019, **36**(5), 529–541.

29 K. Jackson and O. Orekha, Low Density Proppant in Slickwater Applications Improves Reservoir Contact and Fracture Complexity - A Permian Basin Case History, in *SPE Liquids-Rich Basins Conference - North America*, Society of Petroleum Engineers: Midland, Texas, USA, 2017, pp. 1–20.

30 A. Radwan, A Multifunctional Coated Proppant: A Review of Over 30 Field Trials in Low Permeability Formations, in *SPE Annual Technical Conference and Exhibition*, Society of Petroleum Engineers, San Antonio, Texas, USA, 2017, pp. 1–20.

31 A. Neto, F. Prata, J. Gomez, C. A. Pedroso, M. Martins and D. Silva, Ultralightweight Proppants: An Effective Approach To Address Problems in Long Horizontal Gravel Packs Offshore Brazil, *SPE Drill. Completion*, 2013, **27**, 613–624.

32 P. Siddhamshetty, S. Mao, K. Wu and J. S.-I. Kwon, Multi-Size Proppant Pumping Schedule of Hydraulic Fracturing: Application to a MP-PIC Model of Unconventional Reservoir for Enhanced Gas Production, *Processes*, 2020, **8**, 570.

33 S. Jiang, P. Chen, M. Yan, B. Liu, H. Liu and H. Wang, Model of effective width and fracture conductivity for hydraulic fractures in tight reservoirs, *Arabian J. Sci. Eng.*, 2020, **45**, 7821–7834.

34 A. M. Elsarawy and H. A. Nasr-El-Din, A new method to measure propped fracture width and proppant porosity in shale fractures, *J. Pet. Sci. Eng.*, 2019, **181**, 106162.

35 S. Pahari, P. Bhandakkar, M. Akbulut and J. S. I. Kwon, Optimal pumping schedule with high-viscosity gel for uniform distribution of proppant in unconventional reservoirs, *Energy*, 2021, **216**, 119231.

36 A. Katende, L. O'Connell, A. Rich, J. Rutqvist and M. Radonjic, A comprehensive review of proppant embedment in shale reservoirs: Experimentation, modeling and future prospects, *J. Nat. Gas Sci. Eng.*, 2021, 104143, ISSN 1875-5100.

37 N. I. Osuji, J. Zhang and M. D. Tagne, Numerical simulation on the effect of particle shape on mechanical response of proppants in horizontal fractures, *Computational Particle Mechanics*, 2021, 2196–4386.

38 A. A. A. Alzanam, U. Ishtiaq, A. S. Muhsan and N. M. Mohamed, A Multiwalled Carbon Nanotube-Based Polyurethane Nanocomposite-Coated Sand/Proppant for Improved Mechanical Strength and Flowback Control in Hydraulic Fracturing Applications, *ACS Omega*, 2021, **6**(32), 20768–20778.